J Mater Sci (2010) 45:4345–4350
DOI 10.1007/s10853-010-4358-y

EUROMAT 2009

Pressureless infiltration versus wetting in AlSi/graphite system

N. R. Calderon · R. Voytovych · J. Narciso · N. Eustathopoulos

Received: 16 November 2009 / Accepted: 26 February 2010 / Published online: 27 March 2010

Abstract The aim of this investigation is to study the mechanism of spontaneous infiltration of AlSi alloys into porous graphite with emphasis on the role of the reaction of carbide formation in the infiltration process. Results are obtained using the sessile drop technique that enables the variation of the infiltration depth with time to be monitored in situ. In addition to the infiltration data, this method provides quantitative information on wetting thus allowing the values of wetting and infiltration rates measured in the same experiment to be compared.

Introduction

Several studies have been published, concerning the infiltration of porous ceramic preforms by AlSi alloys [1–5]. Due to the absence of wettability, infiltration in these studies has been usually performed under an excess pressure in order to overcome the capillary pressure acting as a barrier at the infiltration front. It has been found that the infiltration depth increases parabolically with time [6, 7] attesting that the infiltration rate is limited by the viscous resistance of the liquid alloy, in agreement with the Washburn model (see below). The case of graphite preforms is of particular interest because AlSi alloys wet carbon, the contact angles being close to 30° [8]. For porous media with cylindrical pores, spontaneous infiltration occurs if the equilibrium contact angle is lower than a threshold angle φ equal to 90°. For real porous solids, calculations give φ values in the range 50–85° depending on the pores shape [9, 10]. Therefore, pressureless infiltration of AlSi alloys into carbon performs is possible. For the AlSi alloys, it is well established that at any temperature there is a critical value x^*_{Si} of silicon mole fraction in the liquid alloy above which silicon reacts with carbon to form silicon carbide (SiC) [3, 11]. For instance, at 1100 °C x^*_{Si} is close to 0.15. For alloys more diluted in Si, the system is still reactive but the reaction product formed at the interface is aluminium carbide (Al_4C_3). In this study, pressureless infiltration experiments are performed with two alloys, Al30 at.% Si and Al40 at.% Si, at temperatures between 1000 and 1125 °C. For these compositions and temperatures SiC is expected to form at the interface. At temperatures lower than 1000 °C, the surface of AlSi droplet is still oxidized, even in high vacuum [12], and the oxide layer covering the surface can hinder the infiltration process. As will be shown later, at temperatures higher than 1125 °C, the stress generated by the formation of the reaction product leads to extensive cracking. It is important to note that as it was found by Jacquier et al. [13] and confirmed in [8], the reactivity between carbon and AlSi alloys decreases with increasing concentration of Si in the alloy.

The dynamics of pressureless infiltration into carbon performs by silicon carbide forming melts was studied previously for pure silicon [14–17] and NiSi alloys [18]. According to [14] the process of infiltration of Si can be described as consisting of a rapid, non-reactive, infiltration followed by the reaction between Si and C to form SiC. The rate of infiltration is assumed to be controlled by the viscous flow of the liquid and the infiltration depth h

N. R. Calderon (✉) · J. Narciso
Departamento de Química Inorgánica, Instituto Universitario de Materiales de Alicante, Universidad de Alicante, Apdo. 99, 03080 Alicante, Spain
e-mail: noelia.rojo@ua.es

R. Voytovych · N. Eustathopoulos
SIMaP/PHELMA, INPG, D.U., St Martin d'Hères, BP 75, 38402, France

varying parabolically with time t according to Washburn's equation [19]

$$h^2 = r_{\text{eff}} \cdot \frac{\sigma \cdot \cos\theta_e}{2 \cdot \eta} \cdot t = r_{\text{eff}} \cdot K \cdot t \quad (1)$$

where σ and η are the surface tension and viscosity of the liquid, θ_e the equilibrium contact angle of the liquid on the solid and r_{eff} an effective pore radius characteristic of the preform [14]. Experimental results obtained recently for the reactive infiltration of NiSi alloys into porous graphite [18] led to a very different description of reactive infiltration. Infiltration in this system does not show a parabolic trend as predicted by Washburn's equation, but is linear in time. Moreover, the activation energy of infiltration is one order of magnitude higher than the activation energy for viscous flow of metallic melts in porous media. Therefore, it was concluded that reactive infiltration is not limited by the viscous flow but by the process at the infiltration front where the formation of the reaction product is coupled with the wetting of the pore walls by the alloy.

The aim of this investigation is to establish the mechanism of spontaneous infiltration of AlSi alloys into porous graphite (C_{gr}) with emphasis on the role of the reaction of carbide formation in the infiltration process. Results are obtained using the sessile drop technique that enables the variation of the infiltration depth with time to be monitored in situ [18]. In addition to the infiltration data, the method provides quantitative information on wetting thus allowing the values of spreading and infiltration rates measured in the same experiment to be compared. The experiments are performed in high vacuum.

Experimental procedure and materials

Infiltration experiments were carried out in a horizontal alumina tube furnace under a static atmosphere in high vacuum ($P < 2 \times 10^{-4}$Pa) by the sessile drop method.

Porous graphite preforms of $5 \times 20 \times 20$ mm^3 used for the infiltration experiments were supplied by Schunk Kolenstofftekcnikk GmHb. These preforms have a geometrical density of 1.39 g/cm^3 and a purity of 99.7%, the remaining 0.3% being hydrogen. The material has an open porosity of 35%, negligible closed porosity (0.07%) and a bending strength of 6 MPa. The degree of graphitization as found by X-ray diffraction was 88%. The pore size distribution determined by mercury porosimetry showed that 95% of pore diameters are in the 1–6 μm range, with a median value of 4 ± 0.2 μm. The effective radius r_{eff}, which may be much lower than the median value [14], was obtained by measuring the infiltration kinetics of an auxiliary, low temperature, non-reactive liquid (polyethylene glycol (PEG)) with known values of surface tension, viscosity and contact angle (Table 1) [11, 20–23]. Using these values and the slope of the straight line expressing the squared infiltration depth as a function of time, r_{eff} was found to be 0.14 μm. The surface condition of preforms measured by a mechanical profilometer shows an average roughness $R_a \approx 3$ μm. Prior to infiltration, porous graphite preforms are treated up to 1200 °C during 30 min in high vacuum in order to remove adsorbed species.

Table 1 Physicochemical properties of AlSi (40 at.% Si) alloy at 1100 °C and of polyethylene glycol (PEG) at room temperature

	Contact angle (deg)	Surface tension (mN/m)	Viscosity (mPa s)
PEG	15 [20]	44 [21]	64 [21]
AlSi	30 [8]	800 [22]	7.0 [23]

The AlSi alloys were prepared in situ during the sessile drop experiment from the pure elements Al (99.9997% purity) and Si (99.9995% purity) supplied by Johnson Matthey. The Si piece was placed over the porous graphite preforms and the Al on top of the Si in order to avoid the contact of the molten Al with the substrate before complete formation of the alloy (Fig. 1).

The temperature cycle consists in an initial heating up to 900 °C at 10 °C/min followed by a faster heating (at 25 °C/min) up the nominal infiltration temperature in order to minimize the time between the complete melting and the holding temperature. The change of the drop shape (having a mass of about 100 mg) with time is monitored by a CCD camera linked to a video recorder. The video system is linked to a computer allowing the contact angle θ, drop base diameter $2R(t)$ and visible drop volume $V(t)$ to be calculated using specific software. The infiltrated volume V_{inf} is calculated as $(V_0 - V(t))$ where V_0 is the initial drop volume. In this way, the height of infiltrated liquid h_L can be deduced, for each increment of time, by dividing V_{inf} by the contact area $\pi R(t)^2$. Then the infiltration depth h is obtained by dividing h_L by the volume fraction of pores α_p. Details of the h_L and h calculation are given in [16] where it is shown that the quantity h_L can be used to determine the general trend of the infiltration curves (linear, parabolic or other). As for the infiltration rate U_{inf}, its average value is more accurately evaluated by $U_{\text{inf}} = h_f^*/t_{\text{inf}}$, where h_f^* is the infiltration depth at the end of the experiment measured directly on metallographic sections (Fig. 2) (the symbol * is used to distinguish it from the calculated infiltration depth h).

Results and discussion

Preliminary experiments performed at 1000 °C with a 30 at.% Si alloy led to a negligible infiltration after 1 h

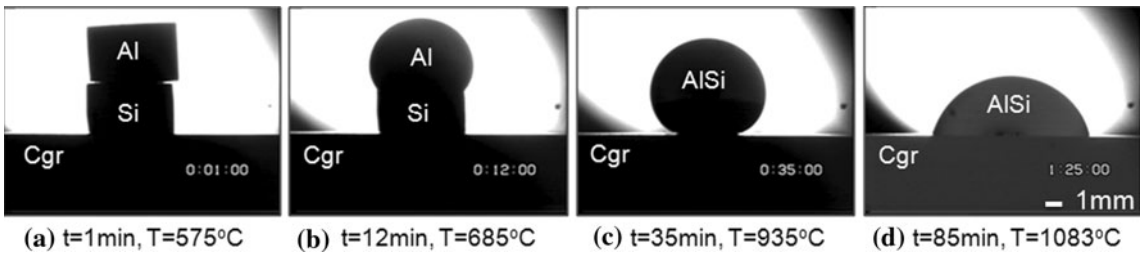

Fig. 1 The different stages of in situ alloy formation and wetting: initial configuration (**a**), Al melting (**b**), drop formation (**c**) and wetting (**d**)

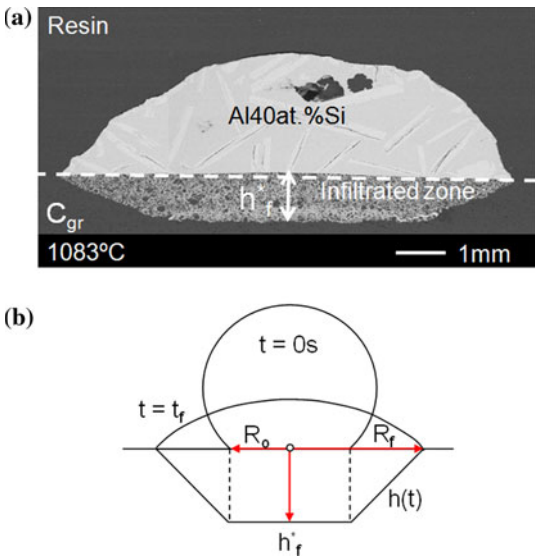

Fig. 2 **a** SEM micrograph of the droplet cross section. Due to stress generated by the reaction the interface is curved. **b** Schematic drawing of the drop with the beginning and the end of the wetting process. The infiltrated zone at the end of the experiment is also given

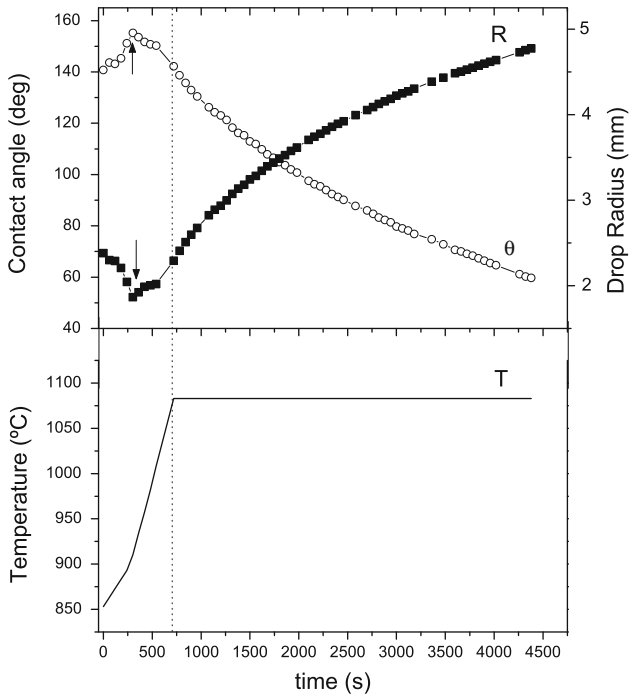

Fig. 3 Evolution of contact angle and drop base radius (*top*) and of temperature (*bottom*) with time for Al40 at.% Si at a plateau temperature of 1083 °C. The *arrows* mark the receding of the liquid drop after formation of the alloy and the dotted line the beginning of the isothermal stage

holding, indicating that at this temperature droplet oxidation prevents infiltration. At 1083 °C, with the same alloy, significant infiltration occurred. However, after 25 min of holding, stress generated by the reaction provoked cracking and detachment of the infiltration zone (several hundred of microns thick) from the graphite bulk. In view of the above results and the findings in the literature about the reactivity between AlSi alloys and graphite (see introduction) next experiments were performed with 40 at.% Si alloys at temperatures in the range 1050–1125 °C.

Wetting

Figure 3 presents the curves $\theta(t)$ and $R(t)$ together with the temperature profile during experiment performed for a holding temperature of 1083 °C. Since the experiment was performed according to the classical sessile drop method, where the alloy and the substrate are in contact during heating, the melting of the drop as well as the beginning of spreading started before the holding temperature was attained. The arrows mark the receding of the liquid drop after the complete formation of the alloy, which is characterized by a sudden increase of the contact angle and a decrease of the drop base radius. Dotted line marks the beginning of the isothermal stage.

The contact angle varies from 155° to the value of 60° observed after 60 min of isothermal hold. However, the angle of 60° is not yet the steady contact angle since the spreading was still occurring at the moment when heating was stopped. (It must be noted that the equilibrium contact angle of AlSi alloys on the reaction product, i.e. on SiC, is close to 30° [24].) During the isothermal stage, spreading occurred with a rate decreasing continuously with time. However, at $\theta < 90^{\circ}$ a quasi-linear spreading is observed where the spreading rate $U_{spr} = dR/dt$ becomes nearly constant and equal to $U_{spr} = 0.36\,\mu m/s$. This value is close

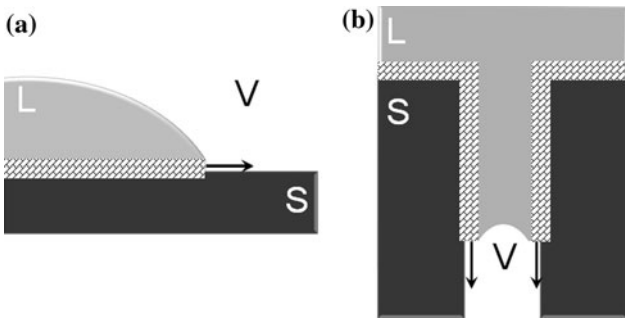

Fig. 4 Schematic representation of reaction-controlled wetting (**a**) and infiltration (**b**) processes. Note that the scales in these two cases are very different, millimetric (**a**) and micronic (**b**). For simplicity purposes, a cylindrical pore is considered

to the spreading rate at the quasi-linear spreading stage measured for AlSi alloys on smooth surfaces of vitreous carbon [8]. Such spreading rates are several orders of magnitude slower than the spreading rates measured previously in non-reactive liquid metal/solid systems [25–27]. Therefore, in agreement with [8], it is concluded that the spreading rate of AlSi on graphite is not limited by the viscous flow of the liquid but by the chemical reaction at the solid–liquid–vapour triple line where the growth of wettable SiC takes place parallel to the liquid/substrate interface (Fig. 4a). In turn, it was shown that this reaction is controlled by the transfer of carbon atoms from the initial substrate to the liquid at the graphite/alloy interface [8].

Infiltration

The variation of drop volume $V(t)$ and infiltrated volume $V_{inf}(t)$ during the infiltration experiment depicted in Fig. 3 together with the temperature profile are presented in Fig. 5. The infiltrated volume $V_{inf}(t)$ is calculated taking for the initial drop volume V_0 the value of drop volume at the beginning of the isothermal stage. The infiltration depth h is calculated from h_L taking $\alpha_p = 0.35$. The infiltration zone under the drop of this experiment is shown in Fig. 2. By comparing the curves of Figs. 3 and 5, it can be seen that infiltration starts when the macroscopic contact angle is as high as 140–150°. It must be emphasized that this contact angle is different from the local contact angle formed on the pore walls at the perform entrance. This local contact angle is expected to attain quasi-instantaneously the equilibrium contact angle θ_e.

These results show that infiltration is not limited by the viscous flow of the alloy into the porous media. Indeed, the infiltration is basically linear with time, i.e. infiltration does not obey the parabolic law of Washburn (Eq. 1). Further evidence is obtained by comparing the experimental infiltration time (3600 s) with the time predicted by Eq. 1 for the same value of h (1 mm). The last time, calculated using

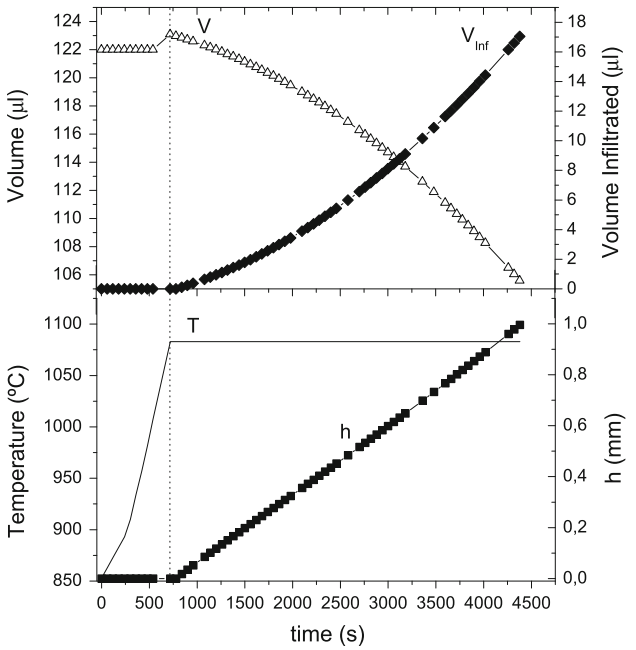

Fig. 5 Infiltration kinetics for Al40 at.% Si at 1083 °C. Evolution with time of drop volume and infiltrated volume (*top*) and of temperature and depth of infiltration (*bottom*) for the experiment given in Fig. 3. The *dotted line* marks the beginning of the isothermal stage

the value $r_{eff} = 0.14$ µm determined with PEG (see "Experimental procedure and materials" section) and physico-chemical properties of the AlSi alloy given in Table 1, is $\sim 10^{-1}$ s. This is four orders of magnitude smaller than the experimental time.

The linearity of $h(t)$ strongly suggests that similarly to the wetting process, infiltration is governed by the reaction of formation of SiC on the pore walls at the infiltration front (Fig. 4b)

Wetting versus infiltration

Reaction-controlled infiltration implies a corresponding activation energy value of the order of some hundreds of kJ/mol, as in reaction-limited wetting [8, 28] whilst control by the viscous flow of AlSi alloys would lead to a value of a few tens of kJ/mol [23]. Table 2 presents results obtained at four temperatures lying between 1065 and 1125 °C. It can be seen that a very limited increase in temperature leads to a strong increase in the infiltration rate (as well as in the spreading rate) corresponding to an activation energy of several hundreds of kJ/mol. However, due to the narrow interval of temperatures explored, an accurate value of the activation energy of infiltration cannot be deduced.

As indicated in Fig. 4, the rate of both infiltration and quasi-linear wetting processes is equal to the growth rate of silicon carbide at the triple line parallel to the graphite

Table 2 Data obtained in the infiltration experiments of porous graphite with Al40 at.% Si at different temperatures

T (°C)	t_{inf} (s)	$h_f^*(\mu m)$	U_{inf} (μm/s)	U_{spr} (μm/s)	U_{inf}/U_{spr}
1065	3100	450	0.15	0.26	0.58
1083	3600	1011	0.28	0.36	0.78
1100	2700	1150	0.43	0.55	0.77
1125	780	1000	1.28	1.15	1.11

t_{inf} infiltration time, h_f^* depth of infiltration, U_{inf} infiltration rate, and U_{spr} spreading rate. (For the values in parentheses, see comments in the text)

surface. Accordingly, the infiltration rate U_{inf} and the wetting rate U_{spr} at a given temperature must be equal or at least of the same order of magnitude. This is confirmed by the experimental values of U_{inf} and U_{spr} showing that the ratio U_{inf}/U_{spr} lies between 0.58 and 1.11 (Table 2). As argued in [16], the departure of U_{inf}/U_{spr} from unity is due to the tortuosity of porous graphite. The tortuosity is defined as the ratio between the real distance covered by a fluid between two points lying inside the porous body and the geometrical distance between these points. The tortuosity is per definition higher than one implying for the ratio U_{inf}/U_{spr} values lower than one. This disagrees with the value 1.11 found for this ratio at 1125 °C. The cause of this disagreement is likely cracking of the infiltration zone and detachment of this zone from the graphite bulk (Fig. 6). These phenomena are due to stress generated by volume change accompanying carbide formation associated with the low mechanical resistance of the graphite used in this study (see also [17]).

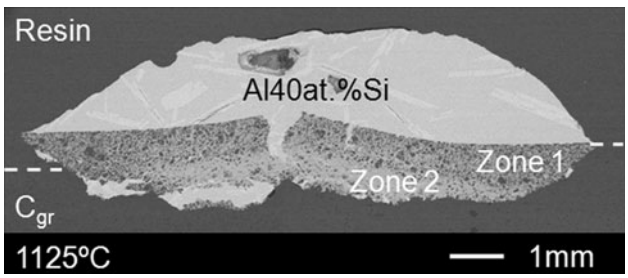

Fig. 6 SEM micrograph of the droplet cross section of graphite infiltrated with Al40 at.% Si at 1125 °C

Infiltration zone: shape and composition

As shown in Fig. 2, the shape of the infiltrated zone is close to a truncated cone. The diameter of the flat bottom of this zone corresponds to the drop base diameter $2R_0$ at the beginning of the infiltration process whilst the upper diameter is equal to the final diameter $2R_F$ of the drop base. For any value of $R < R_0$, the infiltration depth is constant and equal to its highest value because the infiltration time is the largest (3600 s in this experiment). For $R_0 < R < R_F$, the infiltration depth decreases continuously and becomes equal to zero at $R = R_F$ where the infiltration time is equal to zero.

As it can be seen in Figs. 2, 6 and 7 the graphite infiltrated by 40 at.% Si alloy (the same for the 30 at.% Si alloy) consists actually in two zones (noted 1 and 2) with different compositions and graphite conversions. Zone 1, closer to the drop, has a higher content of unreacted graphite. This zone is a graphite/silicon carbide composite containing small quantities of unreacted alloy (Fig. 7). In zone 2, closer to the graphite bulk, almost all the graphite particles were consumed by the reaction. This zone contains both silicon carbide and aluminium carbide (evidenced by EDX micro-analysis) together with unreacted alloy. The formation of aluminium carbide can be explained by the decrease of silicon content in the alloy, due to consumption of this element by the reaction of formation of silicon carbide occurring behind the infiltration front. The presence of an AlSi alloy rich in Al at the infiltration front does not cause a strong change in the spreading rate. For instance, a careful inspection of $h(t)$ curve in Fig. 5 shows that indeed an increase in the slope of $h(t)$ curve occurs above the transition from zone 1 to zone 2 (which takes place for $h \approx 0.7$ mm) but this increase is very slight. This very limited effect of rather large variations in the alloy composition can be understood taking into account the two following conclusions drawn in [8]:

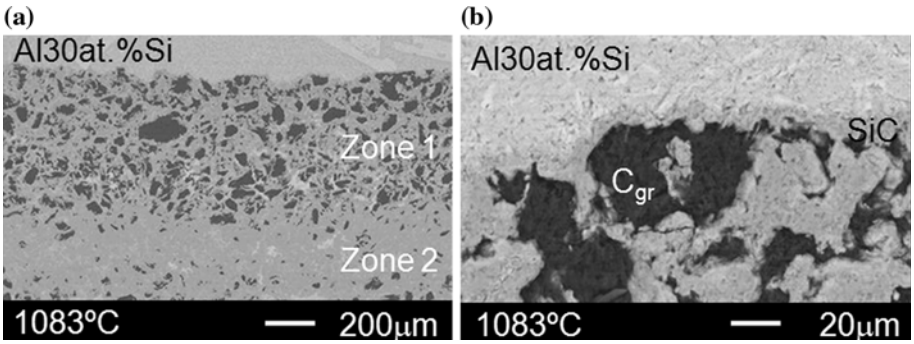

Fig. 7 **a** SEM micrographs of the cross section of Al30 at.% Si/C_{gr} infiltrated at 1083 °C during 27 min. Infiltrated area showing two zones with different conversion of carbon into reaction product. **b** A detail of zone 1 close to the interface

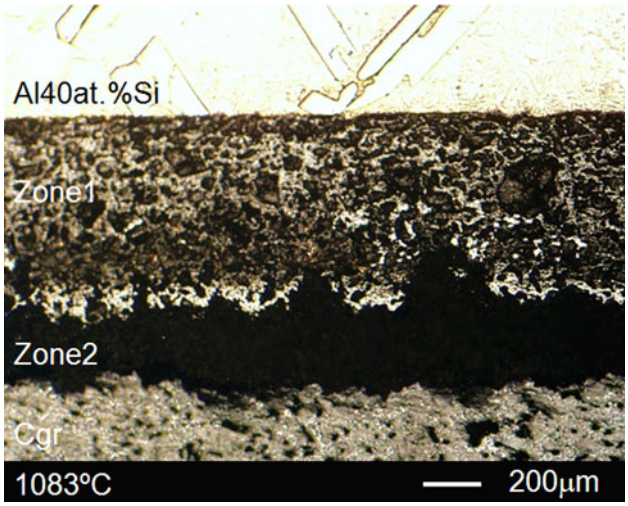

Fig. 8 Aspect of a cross section of a Al40 at.% Si/C_{gr} (60 min at 1083 °C) sample aged 7 months in air. Zone 2 has been removed by hydrolysis of the Al_4C_3 (optical micrograph)

(i) The reaction rate at the triple line is determined by the transfer of carbon atoms at the graphite/alloy interface, i.e. by a process that does not depends directly on the type of carbide (Al_4C_3 or SiC) formed at the interface(although, the type of carbide determines the equilibrium contact angle of the alloy on the graphite), and

(ii) The reaction rate at the triple line depends on the alloy composition weakly (logarithmically).

From the point of view of applications, it is well established that the presence of Al_4C_3 in the composite is detrimental for the mechanical integrity of the material due to the reaction of this carbide with humidity to form CH_4 as is well illustrated in Fig. 8.

Conclusions

Spontaneous infiltration of porous graphite by Al40 at.% Si alloys forming silicon carbide was performed successfully at temperatures in the range 1050–1100 °C under high vacuum conditions. At lower temperatures oxidation of the alloy prevents infiltration whilst at higher temperatures stress generated by the reaction associated with the low mechanical resistance of the graphite used in this study led to extensive cracking. With more resistant graphite preforms higher infiltration temperatures can be used. Consumption of silicon by the chemical reaction behind the infiltration front yields a depletion of Si in the alloy during infiltration resulting ultimately to formation of aluminium carbide, a compound which is detrimental for the mechanical integrity of the composite.

From the point of view of mechanisms, it is concluded that the processes of wetting and infiltration are both governed by the chemical reaction at the triple line. This leads for the drop base diameter and the infiltration depth to linear dependencies with time. Moreover it is shown that the infiltration rate is equal to the spreading rate corrected by a factor taking into account the tortuosity of porous graphite.

References

1. Ejiofor JU, Reddy RG (1997) JOM 49:31
2. Bahraini M, Molina JM, Kida M, Weber L, Narciso J, Mortensen A (2005) Curr Opin Solid State Mater Sci 9:196
3. Narciso-Romero FJ, García-Cordovilla C, Louis E (1992) J Mater Sci Eng B15:148
4. Molina JM, Piñero E, Narciso J, Garcia-Cordovilla C, Louis E (2005) Curr Opin Solid State Mater Sci 9:202
5. Rodriguez-Guerrero A, Molina JM, Rodriguez-Reinoso F, Narciso J, Louis E (2008) Mater Sci Eng A 495:276
6. Mortensen A (2000) In: Kelly A, Zweben C (eds) Comprehensive composite materials, melt infiltration of metal matrix composites, vol 3. Pergamon, Oxford, p 521
7. Garcia-Cordovilla C, Louis E, Narciso J (1999) Acta Mater 47:4461
8. Calderon NR, Voytovych R, Narciso J, Eustathopoulos N (2009) J Mater Sci. doi: 10.1007/s10853-009-3909-6
9. Kaptay G, Barczy T (2005) J Mater Sci 40:2531. doi:10.1007/s10853-005-1987-7
10. Trumble KP (1998) Acta Mater 46:2363
11. Viala JC, Fortier P, Bouix J (1990) J Mater Sci 25:1842. doi: 10.1007/BF01045395
12. Molina JM, Voytovych R, Louis E, Eustathopoulos N (2007) Int J Adhes Adhes 27:394
13. Jacquier C, Chaussende D, Ferro G, Viala JC, Cauwet F, Monteil (2002) J Mater Sci 37:3299. doi:10.1023/A:1016147420272
14. Einset EO (1996) J Am Ceram Soc 79:333
15. Sangsuwan P, Tewari NS, Gatica JE, Singh M, Dickerson R (1999) Metal Mater Trans 30:933
16. Einset EO (1998) Chem Eng 53:1027
17. Israel R, Voytovych R, Protsenko P, Drevet B, Camel D, Eustathopoulos N (2009) J Mater Sci. doi: 10.1007/s10853-009-3869-6
18. Voytovych R, Bougiouri V, Calderon NR, Narciso J, Eustathopoulos N (2008) Acta Mater 56:2237
19. Washburn EW (1921) Am Phys Soc 17:374
20. Calderon NR (2009) PhD Thesis, Alicante
21. Hapgood KP, Litster JD, Biggs S, Howes T (2002) J Colloid Interface Sci 253:353
22. Goicoechea J, Garcia-Cordovilla C, Louis E, Pamies A (1992) J Mater Sci 27:5247. doi:10.1007/BF02403824
23. Battezzati L, Greer AL (1989) Acta Metall 37:1791
24. Ferro AC, Derby B (1995) Acta Met Mater 43:3061
25. Eustathopoulos N, Nicholas M, Drevet B (1999) Wettability at high temperature. Pergamon materials series: vol 3. Pergamon, Oxford
26. Saiz E, Tomsia AP (2004) Nat Mater 3:903
27. Protsenko P, Kozlova O, Voytovych R, Eustathopoulos N (2008) J Mater Sci 43:5669. doi:10.1007/s10853-008-2814-8
28. Bougiouri V, Voytovych R, Dezellus O, Eustathopoulos N (2007) J Mater Sci 42:2016. doi:10.1007/s10853-006-1483-8